Proceedings of International Conference on Heat Exchanger Fouling and Cleaning - 2015 (Peer-reviewed)
June 07 - 12, 2015, Enfield (Dublin), Ireland
Editors: M.R. Malayeri, H. Müller-Steinhagen and A.P. Watkinson
Published online
www.heatexchanger-fouling.com

A FLUID DYNAMIC GAUGING DEVICE FOR MEASURING BIOFILM THICKNESS ON CYLINDRICAL SURFACES

M. Lemos[1,2], S. Wang[1], A. Ali[1], M. Simões[2] and D. I. Wilson[1,*]

[1] Department of Chemical Engineering & Biotechnology, New Museums Site, Pembroke Street Cambridge, CB23RA, UK
*diw11@cam.ac.uk (D.I. Wilson).
[2] LEPABE, Department of Chemical Engineering, Faculty of Engineering, University of Porto, R Dr Roberto Frias, s/n, 4200-465 Porto, Portugal

ABSTRACT

Many industrial processes are susceptible to biofouling. The thickness and structure of such biofilms are key factors in the design of effective cleaning strategies. A novel method based on fluid dynamic gauging has been developed for measuring the thickness and strength of biofilms formed on cylindrical surfaces. The device operates with the test cylinder immersed in liquid: liquid is withdrawn or ejected from a nozzle located near the biofilm surface. There is no net change of liquid volume, making it ideal for sterile and aseptic operation and for studies using valuable liquids. Biofilm removal may also be tested by using appropriate hydrodynamic conditions.

Calibration tests using ejection and suction flows indicated a measurement accuracy of ±19 μm and showed good agreement with computational fluid dynamics simulations. The device was commissioned in tests on *Pseudomonas fluorescens* biofilms formed on high density polyethylene cylinders under conditions of mild shear stress. The biofilm thickness was not uniform: measurements made over the surface of the test cylinders confirmed this.

INTRODUCTION

Biofouling is a costly challenge for many industries. Uncontrolled biofilm accumulation leads to increased energy losses, maintenance and operational costs, and can result in product contamination. Biofouling in pipelines causes reduced flow area, requiring more work to pump liquids along pipelines. Biofilms in heat exchangers decrease heat transfer rates and can also lead to pitting and corrosion failure (Carpentier and Cerf, 1993; Simões and Simões, 2013). In many industries and water treatment stations this problem is mainly countered using biocides, which aim to kill organisms and disinfect surfaces (Flemming, 2011a).

Biofilms grow when there are sufficient amounts of water and nutrients present in the system. There are several mechanisms affecting events at the surface. Particle deposition, controlled essentially by shear stress and temperature, conditions the surface and facilitates the attachment of bacteria. Biological aspects such as species' diversity, their ability to secrete extracellular polymeric substances (EPS), motility and quorum sensing mechanisms also influence the adsorption rate and irreversible adhesion of bacteria to surfaces (Busscher and van der Mei, 1997; Rochex *et al.*, 2008). The EPS matrix acts as a physical barrier to aggressors and delays the diffusion of nutrients and oxygen as well as antimicrobial agents (Flemming, 2011b).

The cells in biofilms differ from their planktonic counterparts: they exist in different metabolic states, are less susceptible to pH and temperature variations (Mah and O'Toole, 2001; Xu *et al.*, 2000), and can differ in their genome following irreversible adhesion (Davies *et al.*, 1998). Biofilms adopt complex structures, with viscoelastic properties, that are resilient to physical changes and chemical agents (Klapper *et al.*, 2002; Xu *et al.*, 2000). Biofilms interact with their surroundings, both the liquid environment and the substrate to which they are attached, and the products of sessile cell metabolism can cause microbially influenced corrosion (Beech and Sunner, 2004; Rochex *et al.*, 2008). Precipitation of minerals can occur, for example the deposition of calcium carbonate by algal biofilms (Mitchell *et al.*, 2010). As a result of the above, biofilms are often highly resistant towards antimicrobial agents: control strategies that rely mainly on biocide action often fail against biofilms, as total inactivation of the microbial cells is rarely achieved. Moreover, when biomass is not completely removed from the surface, there is a greater dispersion of persister cells, causing rapid growth of recidivist biofilms (Lemos *et al.*, 2015b; Simões *et al.*, 2011).

Methods to study biofilms *in situ* are required, and particularly ones which allow the biofilm's response to biocides and other agents to be monitored. This paper reports the development of a variant of the fluid dynamic gauging (FDG) technique for measuring the thickness – and change of thickness in response to biocide application – of biofilms prepared on cylindrical surfaces. The biofilms studied are formed using the rotating cylinder reactor (RCR) developed by the group at Porto. The RCR mimics industrial conditions, with rotation speed being adjusted to create growth conditions with low to moderate shear stress. It has been used previously to form steady-state biofilms, aiming to assess their behaviour and mechanical stability, including the synergic effects of mechanical and chemical stresses in either single as well as multi-species biofilm (Lemos *et al.*, 2015a; Lemos *et al.*, 2015b; Simões *et al.*, 2005; Simões *et al.*, 2009). In this work, biofilms are prepared using the bacterium *Pseudomonas fluorescens,* a species often found in industrial environments due to its short generation time and resistance to heat treatment (Dogan and Boor, 2003). The biofilms are grown on cylinders of high-density polyethylene (HDPE), a polymer regularly used for drinking water pipes (Pelleïeux *et al.*, 2012; Zacheus *et al.*, 2000).

FDG is a non-contact technique developed for measuring the thickness of soft deposits *in situ* and in real

time. Since its introduction by Tuladhar *et al.* (2000) its functionality has been extended to study the strength of soft solid layers using computational fluid dynamics (CFD) to evaluate the stresses that the gauging fluid imposes on the surface being studied (Chew *et al.*, 2004). FDG has been used previously to study biofilms, including algal *Chlorella* (Augustin *et al.*, 2012), cyanobacterial *Synechococcus sp.* WH 5701 (Salley *et al.*, 2012) and bacterial *Escherichia coli* and *Pseudomonas aeruginosa* (Peck *et al.*, 2015) forms, all prepared on flat plates. The device presented here is novel in its use to study biofilms on curved surfaces, and its use of the zero discharge mode introduced by Yang *et al.* (2014). In the latter, alternate ejection and suction stages mean that the total liquid volume does not change over the course of a test. This has particular advantages for aseptic operation or when liquid consumption is to be minimized.

ROTATING BIOFILM REACTOR

Biofilms were formed by *P. fluorescens* ATCC 13525^{T} using the RCR shown in Figure 1, following the methodology described by Lemos *et al.* (2015b). The RCR is an aerobic bioreactor which operates in steady state: three test cylinders are rotated at the same fixed speed, with their axes vertical. The cylinders used in these tests were made from HDPE with diameter 2.5 cm and length 5.0 cm. A thin strip of aluminum foil is attached vertically to the cylinder for checking the alignment when mounted in the FDG system. The gauging nozzle is moved towards the cylinder and contact between the nozzle and the foil completes an electrical circuit. The foil strip is not needed when the cylinder is made from conductive materials such as steel.

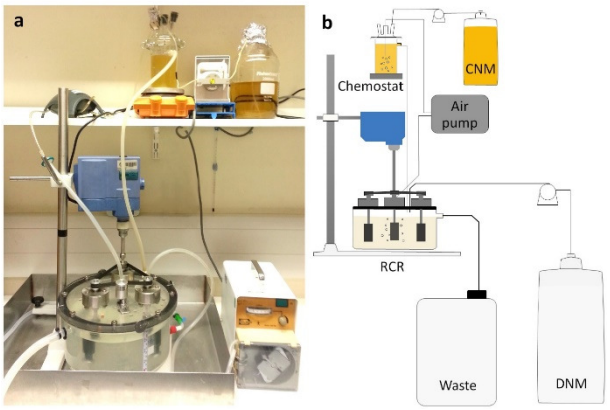

Fig. 1 Photograph (a) and schematic (b) of the rotating fluid reactor apparatus.

The cylinders were removed after a 7 day growth period. The biofilm was scraped from all surfaces apart from the cylinder wall and the samples were weighed before gauging. This process was performed as quickly as possible to prevent drying of the biofilm. The biofilm wet mass was determined by the difference between the mass of the cylinder covered with biofilm and the mass of the clean cylinder. Before FDG measurement, the biofilm was removed from the area of the metallic strip, and for 3 other vertical strips, using cotton swabs. This was done to allow calibrations to be repeated and to check that the cylinder is correctly aligned.

CYLINDRICAL ZERO-DISCHARGE FDG

The device operates in 'pressure mode'. The mass flow rate through the nozzle, $\dot{m}$, is very sensitive to the pressure drop across the nozzle, ΔP, and the distance between the nozzle and the surface, the clearance, h, shown in Figure 3. The mass flow rate is maintained constant, using a syringe pump, and ΔP is measured as the nozzle is moved towards the surface. The measurements of $\dot{m}$ and ΔP are presented as the discharge coefficient, C_{d}, which is the ratio between the measured and the ideal mass flowrate through the nozzle, (Tuladhar *et al.*, 2000):

$$C_{\mathrm{d}} = \frac{\dot{m}}{\pi/4\, d_{\mathrm{t}}^2 \sqrt{2\rho\Delta P_{12}}} \qquad (1)$$

Here d_{t} is the nozzle throat diameter and ρ is the density of the gauging liquid. Knowledge of C_{d} allows h to be estimated from calibration plots. Examples are given in Figure 7(b), where h is plotted as h/d_{t} (d_{t} is the nozzle throat diameter). C_{d} is usefully sensitive to h/d_{t} when $h/d_{\mathrm{t}} < 0.3$. The nozzle location relative to the substrate, h_0, is known from independent measurements (here, the linear slide travel along with the zero/contact measurement). Liquid is either sucked or ejected from the nozzle and ΔP measured, allowing h to be estimated. The thickness of any layer present, δ, is given by:

$$\delta = h_0 - h \qquad (2)$$

In FDG measurements the gauging fluid is in the laminar or inertial regime so the C_{d}- h/d_{t} relationship is sensitive to the Reynolds number, Re_{t}, which is conventionally based on the nozzle throat diameter, d_{t}.

Figure 2 shows a photograph and schematic of the czFDG apparatus. An aluminum frame holds the motorized linear drive and the reservoir (R). The test cylinder is located in a stainless steel shaft, so that its axis is collinear with that of the reservoir. Rotational and vertical movements of the sample are controlled manually, with 12 azimuthal positions at each of 5 heights.

The gauging tube was moved via a motorized linear slide (Zaber Technologies, T-LSR075B, UK), manipulated via LabVIEW™ software (version 2013), with an accuracy of ± 15 µm. Pressure was measured using a piezo pressure transducer (Honeywell 24PCEFA6G, UK) in reference to the atmospheric pressure. Its analog signal was converted to digital via a DAQ device (National Instruments, USB-6009). Data were collected on a laptop using the LabVIEW™ software. The flow of the liquid through the nozzle was set by a syringe pump (Cole-Parmer, EW-74900-20) with stated accuracy of ± 0.5%. An electrical circuit was used to determine the point of zero clearance. A digital microscope (Maplin, UK) provided images of the gauged area with 400× magnification. Figure 3 shows the details of the nozzle and its dimensions.

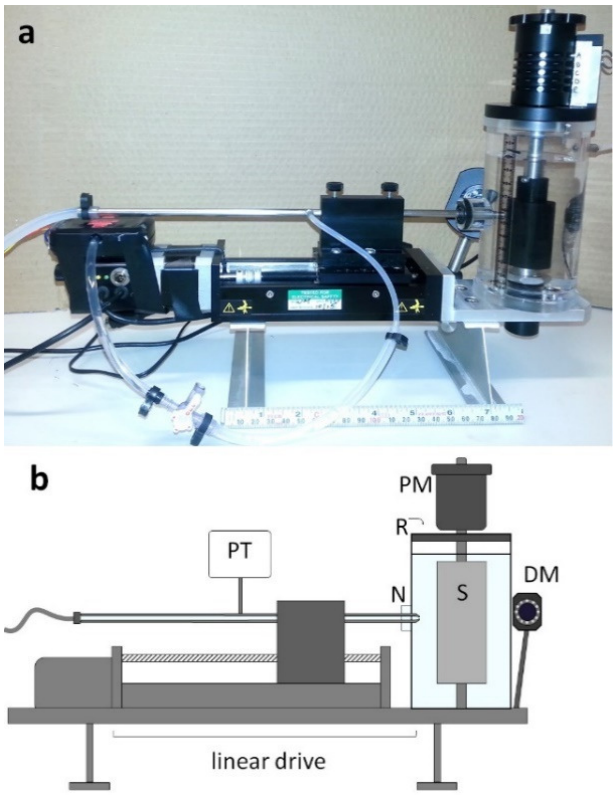

Fig. 2 Photograph (*a*) and schematic (*b*) of the fluid dynamic gauging apparatus. DM - digital microscope; N - nozzle; PM - positioning mechanism; PT – pressure transducer; R - reservoir; S - sample.

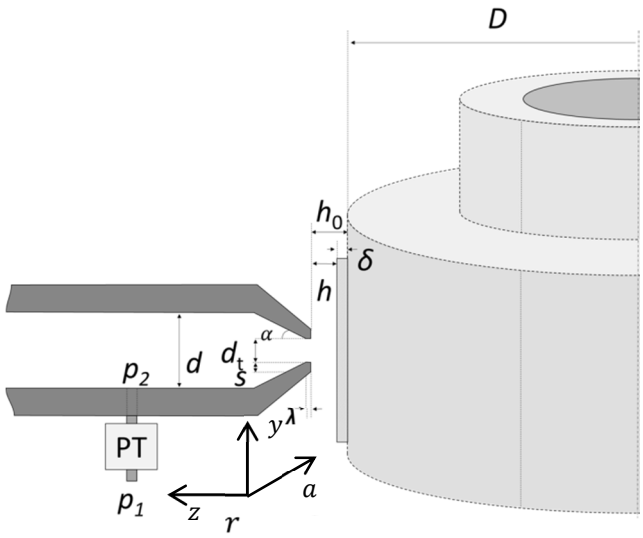

Fig. 3 Detailed schematic of the gauging nozzle. $d_t = 1$ mm, $d = 3.8$ mm, $\lambda = 0.2$ mm, $s = 0.4$. The internal divergent angle, α, is 45°. PT - pressure transducer, δ – deposit thickness; h_0 is the distance between the nozzle and the substrate; h is the clearance measured by FDG.

For calibration tests, both ejection and suction modes were performed with fixed flow rates of 0.066 g/s ($Re_t = 84$) and 0.050 g/s ($Re_t = 63$). The nozzle was moved to a known location relative to the surface and the syringe pump set to eject or withdraw liquid at a constant rate. The pressure drop was measured before, during, and after the flow step in order to determine the static and dynamic pressure drops. The experiments reported here used an absolute pressure transducer so the gravitational contribution had to be accounted for. The nozzle was then moved to give another clearance value and the measurement repeated. This process was automated: adjusting the position of the sample in order to measure at another point on the surface was done manually. The nozzle was moved away from the surface while the cylinder position was adjusted.

Biofilm measurements were performed at room temperature, using phosphate buffer as the gauging fluid, in order to maintain the physiological conditions similar to that in the RCR. Low gauging flow rates, 0.066 g/s and 0.050 g/s, were used to prevent disruption of the biofilm layers. The procedure used for calibration was used to gauge the biofilms at three different heights and four diametrically opposed azimuthal positions.

NUMERICAL SIMULATIONS

Computational fluid dynamics (CFD) simulations were performed using the COMSOL Multiphysics® (version 4.1, Chemical Engineering module) software on a desktop PC. The CFD work employed the techniques described in detail by Chew *et al.* (2004) for flat substrates and by Gu *et al.* (2009) for annular geometries similar to the czFDG. Flow in the tube was assumed to be laminar, steady state and fully established. The gauging liquid was Newtonian and the flow was isothermal. The Navier-Stokes and continuity equations were solved for a set flow rate into or out of the nozzle (for suction and ejection, respectively). The pressure field solution gave an estimate of ΔP, and thus C_d, for comparison with experimental data. The geometry of the model and coordinate system are presented in Fig. 4. The two projections employed in presenting the results are shown in Figure 6(*c*).

Tags A-D label boundaries in the simulation with the following boundary conditions (see (Chew *et al.*, 2004):

A. *Axis of symmetry*

There was no flow across symmetry planes, *i.e.* $\mathbf{n} \cdot \mathbf{v} = 0$, where $\mathbf{n}$ is the vector normal to the relevant plane.

B. *Gauging tube: inlet (ejection flow) or outlet (suction flow)*

Flow is assumed to be fully developed, giving the Hagen-Poiseuille velocity profile, i.e. $v_y = 0$ and

$$v_z = v_{max}\left(1 - \frac{4y^2}{d^2}\right) \quad (3)$$

C. *Walls*

There is no slip at the walls and the walls are impermeable, *e.g.* for the cylinder wall in Fig. 4, $v_y = 0$ and $v_z = 0$.

D. *Bulk liquid in reservoir: outlet (ejection) or inlet (suction)*

The distance of this boundary to the axis of symmetry was set to be much larger than the radius of the gauging tube (d/2). This guarantees that the streamlines are parallel and normal to the boundary surface (Chew *et al.*, 2004).

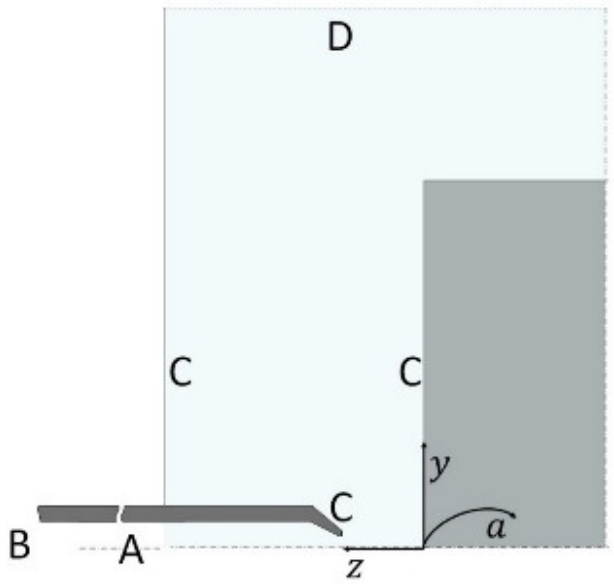

Fig. 4 Simulation geometry. Co-ordinates: z – horizontal axis (gauging tube), y – vertical axis (reservoir height) and a – arc length, along the cylinder surface.

COMSOL uses the finite element method (FEM) to solve the partial differential equations arising from the CFD problem. The domain was modelled using a mesh of tetrahedral elements (see Figure 5), constructed with the software's built-in mesh generator. The mesh density is higher under the nozzle rim and along the lip, where the largest pressure and velocity gradients were found.

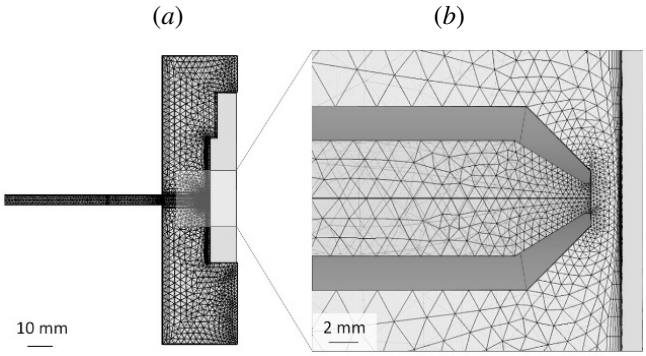

Fig. 5 Simulation mesh, tetrahedral elements. (a) whole system, 2-D slice; (b) detailed illustration of the region beneath the nozzle rim.

The effect of the number of mesh elements, N_e, on the simulation results is reported in Table 1 for a representative case. C_d approaches an asymptote as N_e increases. The asymptote differed for suction and ejection modes. The mesh density affected the numerical performance, *e.g.* time to converge, but the mass balance was closed with accuracy similar to earlier studies (e.*g.* Chew *et al.*, 2004) for even the smallest N_e values. CFD simulation results presented in subsequent sections were generated with the 787334 element mesh as this was judged to give sufficiently good accuracy for reasonable effort.

Table 1. Effect of mesh refinement on solution accuracy for the case Re_t=84, $h/d_t = 0.074$

N_e	Ejection mode		Suction mode	
	C_d	solution time (s)	C_d	solution time (s)
80669	0.127	293	0.121	381
84288	0.126	303	0.121	400
136422	0.126	519	0.121	673
248736	0.125	836	0.121	1089
787334	0.121	2253	0.118	2869
3572597	0.120	17635	0.117	20697

RESULTS AND DISCUSSION

CFD and calibrations

Figure 6 presents velocity distributions within the nozzle for (a) ejection and (b) suction mode for the same Re_t and h/d_t values. The largest velocity gradients are found near the nozzle throat, as reported in previous quasi-static FDG studies (Ali *et al.*, 2013; Gu *et al.*, 2009).

The two flow configurations differ in the existence of large recirculation cells downstream of the nozzle in suction mode, marked by a dashed box in Figure 6(b). For ejection mode the flow in this region approximates a radially converging flow. It is shown in Figure 7 that this gives rise to slightly different C_d behavior in ejection and suction. The patterns also differ in the region between the nozzle rim and the surface, marked by a solid box in Figure 6(ii). In ejection mode, there is a small recirculation zone attached to the underside of the nozzle, which is absent in the suction pattern. This feature gives rise to different shear stress distributions on the substrate surface, shown in Figure 8.

Figure 7 compares the measured pressure drops and the associated C_d values obtained from ejection mode calibration tests using two mass flow rates (0.066 and 0.05 g/s). Plotted alongside are the results from CFD simulations: each CFD datum required a new simulation. Similar trends, and similarly good agreement between experimental and simulation results, were obtained for suction mode. Ejection mode results are presented here as this was the configuration employed to measure the biofilm thickness. It should be noted that there are no adjustable parameters in the CFD calculations. Table 1 shows that the C_d value depends on mesh refinement, and the asymptotic values are plotted.

The calibration curves indicate a usefully linear region for the thickness measurements within the interval $0.05 < h/d_t < 0.25$. For $h/d_t < 0.05$, C_d is small but also very sensitive to any misalignment between the nozzle and the cylinder so that the surfaces are not parallel. This is nullified by avoiding small clearances. The pressure drop is also large when h/d_t is small, requiring a pressure transducer with a large sensitivity range. Furthermore, the high pressure drop means that the approach to the surface is readily noticed and this can set an alarm in the FDG software.

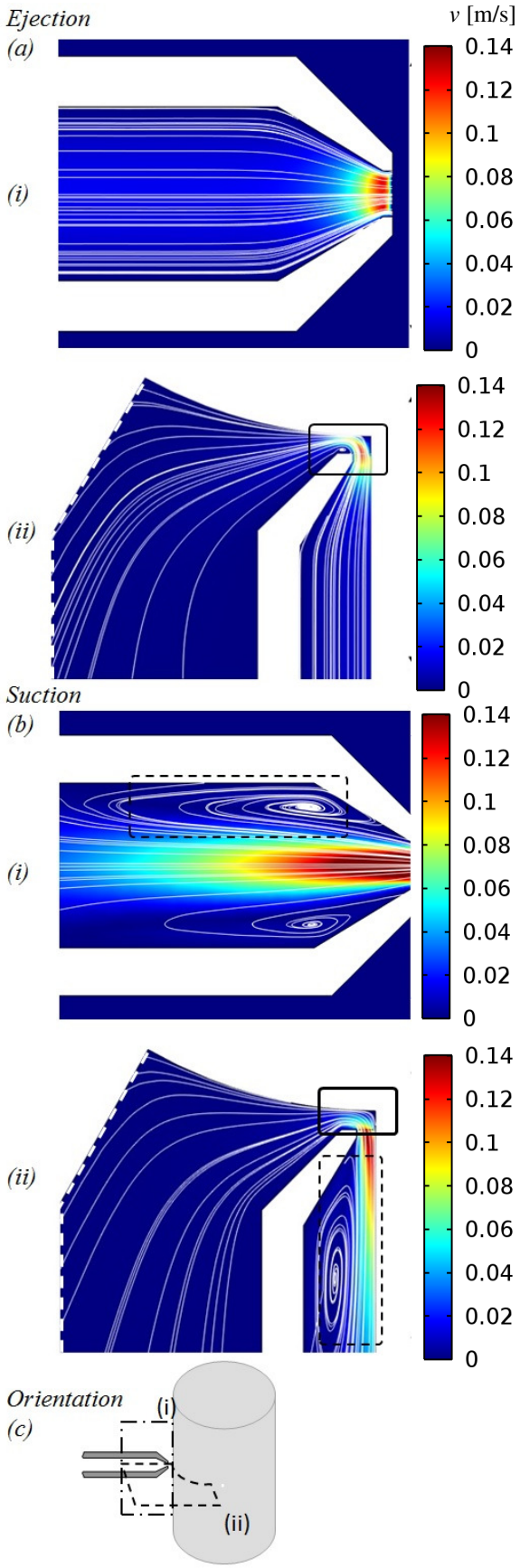

Fig. 6 CFD simulation results for (*a*) ejection and (*b*) suction mode for Re_t=211, h_0= 0.2 mm (h/d_t = 0.2) for the planes labelled (*i*) and (*ii*) in schematic (*c*). Colour scale on right shows velocity scale. Dashed boundary in (ii) shows cropping to fit the space.

For $h/d_t > 0.25$, C_d approaches as asymptote, and an associated small pressure drop. Even if these pressure differences could be measured reliably, the resolution of the device will be poor compared to measurements in the linear interval identified above.

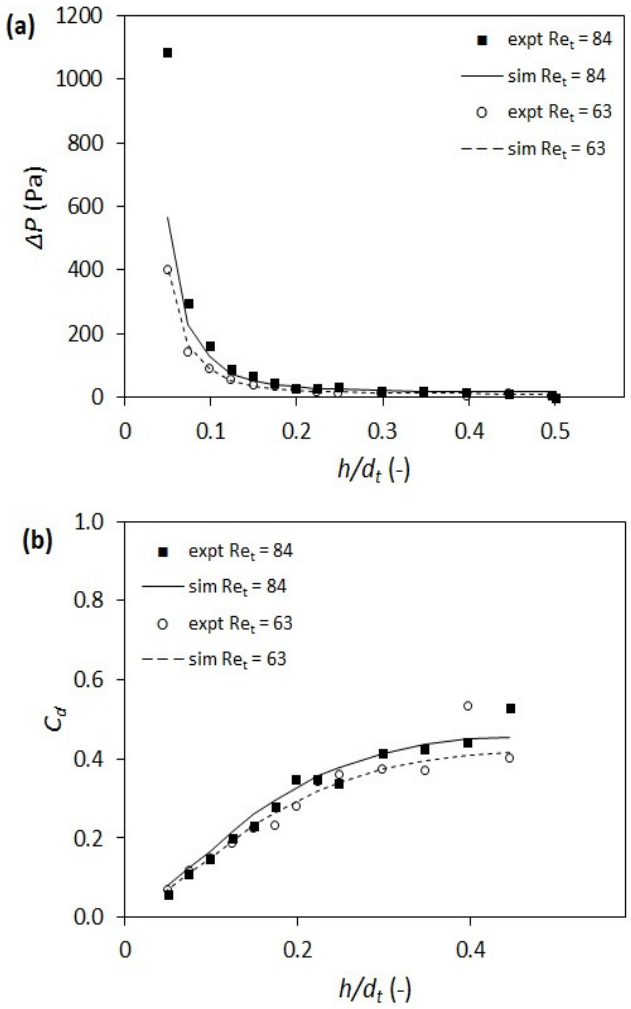

Fig. 7. Comparison of experimental (expt) calibration curves with results obtained by simulation (sim) for ejection mode with Re_t = 84 and Re_t = 63.

The shear stress imposed by the gauging flow on the cylinder surface along the line of increasing *y* co-ordinate is plotted for suction and ejection modes in Figure 8. The system is symmetrical: ejection is plotted with positive *y* and suction with negative *y*.

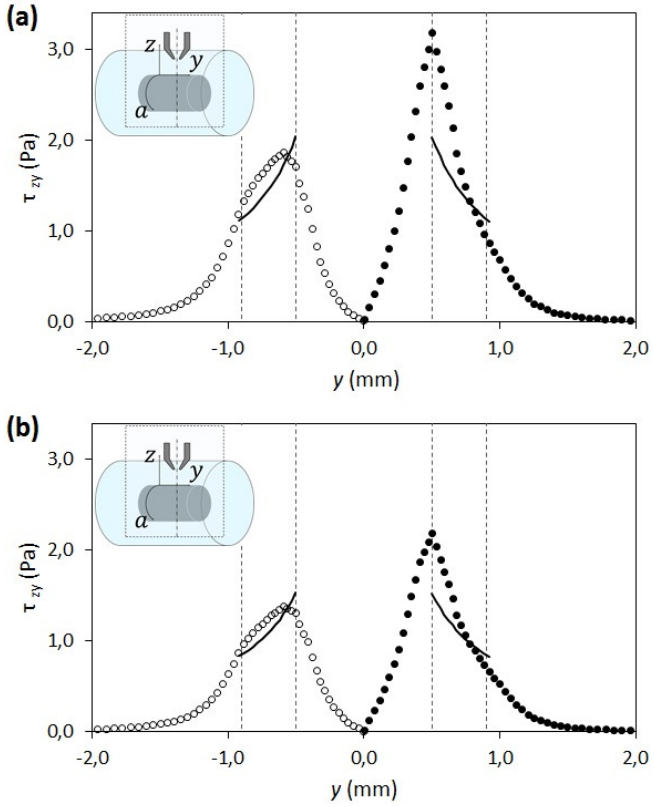

Fig. 8 Shear stresses imposed by the gauging flow on the surface of the cylinder, along the line of increasing y (see insets). (*a*) Re_t = 84, (*b*) Re_t = 63, $h/d_t = 0.25$. Solid symbols - ejection mode, open circles - suction mode. Solid line shows analytical result for parallel discs (Equation (4)). Vertical dashed lines indicate the location of the inner and outer lip of the nozzle.

Figure 8 shows noticeable differences between the two configurations. There is a noticeably larger peak in the shear stress near the nozzle inlet with ejection mode at Re_t = 84, which results from the presence of the recirculation zone attached to the nozzle lip in Figure 6(*a*,*ii*): the exiting liquid has to pass through a narrower channel, increasing the shear rate on the surface and hence the shear stress. This feature is not so marked at the lower flow rate, where there is a smaller recirculation zone. This behavior is also evident when the data are compared with the analytical result for the shear stress distribution created by steady, incompressible radial flow of a Newtonian fluid between two parallel discs (Middleman (1998):

$$\tau = \left(\frac{3\mu\dot{m}}{\rho\pi h^2}\right)\frac{1}{y} \qquad (4)$$

Here y is the distance from the nozzle axis. The corresponding loci are plotted in Figure 8. The magnitudes of the suction simulation results are similar to those predicted by Equation (4), but do not agree exactly. One of the reasons for this is that the flow pattern is not one-dimensional: the gap between the nozzle lip and the surface varies with azimuthal angle (it increases steadily in the *a* direction). This result indicates that Equation (4) can be used to estimate the shear stress imposed on the cylindrical surface or any biofilm growing on it, to one significant figure. Significantly better agreement is obtained for gauging on flat surfaces (Yang *et al.*, 2014). Equation (4) assumes a steady velocity profile in the gap between the discs, which differs from that predicted by the CFD studies for ejection with Re_t = 84. The simulation shear stress value is larger than that predicted, as expected.

It is noteworthy that the shear stress values imposed by the gauging flow on the surface in the region under the nozzle in Figure 8 range from 1-2 Pa when h/d_t = 0.25. The shear stresses imposed by steady pipe flow are given by $\frac{1}{2}C_f \rho u_m^2$, where u_m is the mean bulk velocity and the friction factor, C_f, is typically around 0.005. This gives $\tau \sim 2.5\ u_m^2$, *e.g.* $\tau \sim 2.5$ Pa for u_m = 1 m s^{-1}. The gauging flow is therefore accessing pipe flow conditions even at this low mass low rate. The shear stress can be increased by moving the nozzle closer to the surface: Equation (4) indicates that $\tau \sim h^{-2}$ so at the lower limit of the linear range, h/d_t = 0.05, a shear stress of around 50 Pa can be generated, which would correspond to $u_m \sim 4.5$ m s^{-1}.

The above results demonstrate that zero net flow FDG can be achieved with cylindrical geometries. Measurements of biofilm thickness could be made during an ejection step, a suction step, or both, as the syringe moves from full to empty, empty to full, or back and forth with small volume changes and suction steps. In the tests here with biofilms, thickness measurements were made in ejection mode as the biofilms were quite fragile and could be dislodged as clumps which, in suction mode, could block the nozzle. If this did occur in practice, the pressure drop characteristics would change noticeably. The nozzle would be withdrawn a long distance from the test surface and a fast burst of liquid ejected in order to clear the nozzle.

Measurements on biofilms

The photographs of biofilms formed on an HDPE cylinder after 7 days of growth in Figure 9 show uneven coverage, with cells adopting striation patterns. These patterns appeared to follow machining marks in the HDPE surface which may have functioned as harbours for initial cell adhesion (Whitehead and Verran, 2006).

(*a*) (*b*)

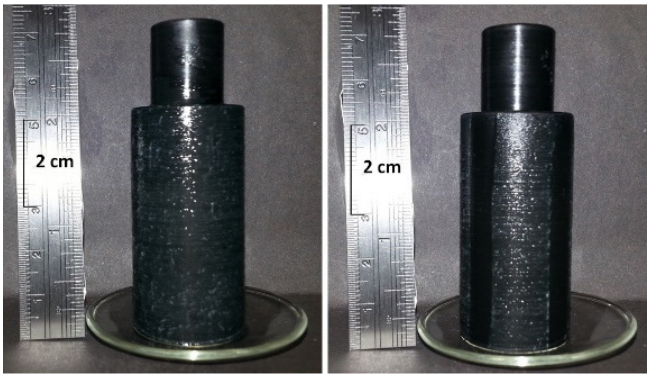

Fig. 9 HDPE samples (*a*) recovered from the RCR, and (*b*) before FDG testing (biofilm has been removed from the ends and calibration zones cleaned).

Biofilm thicknesses measured on three different cylinders after three tests are plotted in Fig.10. The average wet mass in these cases was 20.0 ± 2.2 $mg_{biofilm}$ cm^{-2}. Measurements were made at 12 positions for each cylinder. There is noticeable variation between cylinders and between tests. The resolution of the czFDG technique with the pressure transducer used here was ±23 µm. The uncertainty of the czFDG measurements on clean substrates was ±19 µm, with the largest source of error being the accuracy of the linear slide.

The pattern obtained for cylinder 2 in Tests A and B was noticeably different to cylinders 1 and 3, which showed reasonably similar trends. Test C was noticeably different from the previous cylinders. The absence of a measurement on cylinder 2 in these tests does not indicate that there was no layer present: the resolution of ±23 µm is quite large compared to the size of individual *P. fluorescens* cells, which are rod shaped with a typical diameter of 2 µm.

The digital microscope confirmed that material was present on the surface, but evidently some factor had prevented the bacteria progressing to the colonization and growth stage. If anything, these results confirm some of the difficulties in working with biofilms: reproducibility is hard to achieve! In fact, the non-uniformity in biofilm thickness is one of their natural characteristics. Phenotypic heterogeneity and differentiation of cells, oxygen and nutrient gradients and different genetic pathways contribute to complex spatial arrangements of the cell clusters (de Beer *et al.*, 1994; Stewart, 2003; Stewart and Franklin, 2008), and consequently influence the architectural structure of the EPS matrix, giving non-uniform biofilms.

The values in Figure 10 agree with results obtained for the same species on HDPE in Porto (data not reported, to be published) and with results obtained for biofilms formed on stainless steel by *Bacillus cereus*, under similar hydrodynamic conditions (Lemos *et al.*, 2015b), measured using a contact technique based on a digital micrometer.

Augustin *et al.* (2012) reported similar variation in thickness values for *Chlorella* biofilms, measured with scanning FDG operated with under mass flow mode, where the pressure drop is fixed and the mass flow rate varies as the nozzle approaches the surface (as used by Tuladhar *et al.*, 2000). Salley *et al.* (2012) measured the thickness of biofilms formed from *Synechococcus sp.* WH 5701 on different substrates (glass, stainless steel and indium tin oxide), over a period of 4 weeks. They measured thickness at three positions on each substrate and reported variation similar to that on cylinders 1 and 3 in tests A and B. These algal biofilms grew to thicknesses ranging from 100-300 µm after 4 weeks. The variation between measurements decreased with time, as the biofilms became more mature.

Previous studies using FDG techniques also reported noticeable variation in thickness for biofilms: Augustin *et al.* and Salley *et al.* used static growth conditions, whereas Peck *et al.* (2015) grew *Escherichia coli* and *Pseudomonas aeruginosa* on different substrates, placed in petri dishes and cultivated in a rocking incubator with an agitation speed of 70 rpm. All the above studies employed flat substrates: to our knowledge, this is the first work reporting results for steady-state bacterial biofilms formed on curved surfaces, under rotational flow. The ability of the czFDG to scan over the entire cylinder surface also allows meaningful statistics to be collected for each sample.

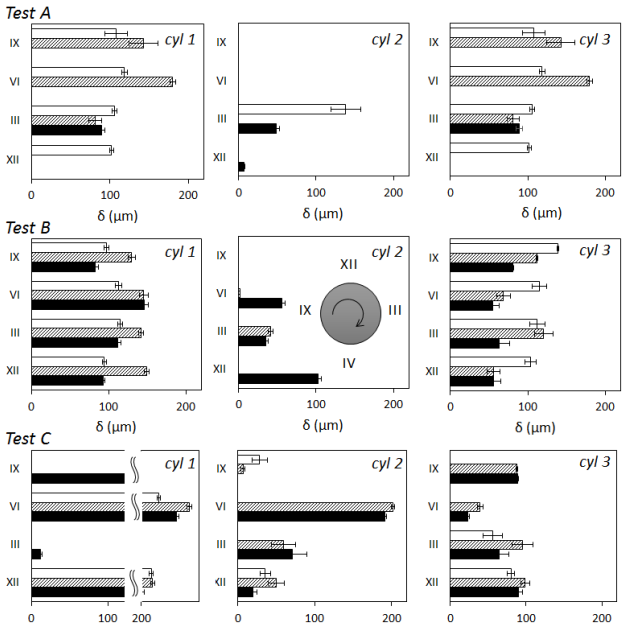

Fig. 10 Biofilm thickness measurements for three different cylinders (labelled 1, 2 and 3) after three tests (labelled A, B and C). Measurements performed at 4 different azimuthal positions (indicated in Roman numerals, corresponding to clock positions, see middle plot) and 3 different heights (open bar - highest position, crossed bar - intermediate position, solid bar - lowest position). Error bars indicate the uncertainty calculated for measurements at that location.

This paper demonstrates proof-of-concept for the czFDG device for measuring the thickness of soft layers on cylindrical surfaces in situ and in liquid resembling their native environment. The device has employed to obtain data for biofilms grown on HDPE surfaces. Tests on other surfaces, including stainless steel and glass, are ongoing.

The device allows real time thickness measurement and visualization of removal of the layer, which is not reported here. The CFD simulations allow adhesive or cohesive removal to be related to absolute values of the shear stress imposed by the gauging liquid. The technique can be used to monitor the thickness and strength of the biofilms as the liquid is changed to one including microbial agents.

One aim of the RCR/czFDG system is to determine the extent to which biofilm growth conditions affect their thickness, adhesive and cohesive strengths, and also their internal diffusivity and eventually resistance to antimicrobial agents (Melo, 2005).

CONCLUSIONS

1. A novel FDG device for measuring the thickness and strength of soft deposits on cylindrical surfaces, with zero discharge of liquid from the system, was designed, constructed and commissioned. *Pseudomonas fluorescens* biofilms formed under mild shear stress on HDPE cylinders in the rotating cylinder bioreactor were successfully measured with this device, under aseptic conditions.
2. The alignment of samples is essential for obtaining accurate measurements, and the calibration must be performed using the test sample in place. Further developments of the device include automation of the cylinder positioning.

ACKNOWLEDGMENTS

The authors acknowledge the financial support provided by the Operational Programme for Competitiveness Factors – COMPETE and by FCT – the Portuguese Foundation for Science and Technology through Project Bioresist – PTDC/EBB-EBI/105085/2008 and SFRH/BD/79396/2011 (Madalena Lemos). Funding for some of the czFDG components was provided by the Royal Society's Paul Instrument Fund. An EPSRC PhD studentship for Akin Ali, and funding from Fitzwilliam College for Shiyao Wang, is also gratefully acknowledged.

NOMENCLATURE

Roman

a	arc length (m)
A	dimensionless *a*-coordinate
C_d	discharge coefficient (-)
C_f	friction factor (-)
d	inner diameter of dynamic gauging tube (m)
d_t	nozzle throat diameter (m)
D	diameter of liquid reservoir (m)
g	acceleration due to gravity (m s^{-2})
h	clearance between nozzle and gauging surface (m)
h_0	clearance between nozzle and gauging surface (m)
$\dot{m}$	tube discharge mass flow rate, kg/s
$\mathbf{n}$	normal vector of the relevant plane
N_e	number of mesh elements
p_i	pressure (Pa)
ΔP	pressure drop (Pa)
Re_t	Reynolds number at the throat of the nozzle (-)
s	lip width (m)
u_m	bulk mean velocity (m s^{-1})
$\mathbf{v}$	velocity vector
v	velocity (m s^{-1})
x	horizontal coordinate (m)
y	vertical coordinate

Greek

δ	thickness of measured layer (m)
λ	nozzle entry length (m)
θ	nozzle angle (–)
μ	fluid viscosity (Pa s)
ρ	fluid density (kg m^{-3})
τ	wall shear stress (Pa)
τ_{rz}	wall shear stress on *x*-plane in the *y*-direction
$\tau_{r\theta}$	wall shear stress on *x*-plane in the *a*-direction

Acronyms

CFD	computational fluid dynamics
czFDG	cylindrical zero-discharge fluid dynamic gauging
FEM	finite element method

REFERENCES

Ali, A., Chapman, G.J., Chew, Y.M.J., Gu, T., Paterson, W.R. and Wilson, D.I., 2013. A fluid dynamic gauging device for measuring fouling deposit thickness in opaque liquids at elevated temperature and pressure. *Exp Therm Fluid Sci*, 48(0): 19-28.

Augustin, W., Chew, Y.M.J., Gordon, P.W., Lister, V.Y., Mayer, M., Paterson, W.R., Peralta, J.M., Scholl, S. and Wilson, D.I., 2012. Dynamic gauging of soft fouling layers on solid and porous surfaces. *Chem Ing Tech*, 84(1-2): 46-53.

Beech, I.B. and Sunner, J., 2004. Biocorrosion: towards understanding interactions between biofilms and metals. *Curr Opin Biotech*, 15(3): 181-186.

Busscher, H.J. and van der Mei, H.C., 1997. Physico-chemical interactions in initial microbial adhesion and relevance for biofilm formation. *Adv Dental Res*, 11(1): 24-32.

Carpentier, B. and Cerf, O., 1993. Biofilms and their consequences, with particular reference to hygiene in the food industry. *J Appl Microbiol*, 75(6): 499-511.

Chew, J.Y.M., Cardoso, S.S.S., Paterson, W.R. and Wilson, D.I., 2004. CFD studies of dynamic gauging. *Chem Eng Sci*, 59(16): 3381-3398.

Davies, D.G., Parsek, M.R., Pearson, J.P., Iglewski, B.H., Costerton, J.W. and Greenberg, E.P., 1998. The involvement of cell-to-cell signals in the development of a bacterial biofilm. *Science*, 280(5361): 295-298.

de Beer, D., Stoodley, P., Roe, F. and Lewandowski, Z., 1994. Effects of biofilm structures on oxygen distribution and mass transport. *Biotechnol Bioeng*, 43(11): 1131-1138.

Dogan, B. and Boor, K.J., 2003. Genetic diversity and spoilage potentials among *Pseudomonas* spp. isolated from fluid milk products and dairy processing plants. *Appl Environ Microb*, 69(1): 130-138.

Flemming, H.-C. (2011a) Microbial Biofouling: Unsolved Problems, Insufficient Approaches, and Possible Solutions. In: Biofilm Highlights. Flemming, H.-C., Wingender, J. and Szewzyk, U. (eds), pp. 81-109, Springer Berlin Heidelberg.

Flemming, H.C., 2011b. The perfect slime. *Colloids and surfaces. B, Biointerfaces*, 86(2): 251-259.

Gu, T., Chew, Y.M.J., Paterson, W.R. and Wilson, D.I., 2009. Experimental and CFD Studies of Fluid Dynamic Gauging in Annular Flows. *AlChE J*, 55(8): 1937-1947.

Klapper, I., Rupp, C.J., Cargo, R., Purvedorj, B. and Stoodley, P., 2002. Viscoelastic fluid description of bacterial biofilm material properties. *Biotechnol Bioeng*, 80(3): 289-296.

Lemos, M., Gomes, I., Mergulhão, F., Melo, L. and Simões, M., 2015a. The effects of surface type on the removal of *Bacillus cereus* and *Pseudomonas fluorescens* single and dual species biofilms. *Food Bioprod Process*, 93(0): 234-241.

Lemos, M., Mergulhão, F., Melo, L. and Simões, M., 2015b. The effect of shear stress on the formation and removal of *Bacillus cereus* biofilms. *Food Bioprod Process*, 93(0): 242-248.

Mah, T.F.C. and O'Toole, G.A., 2001. Mechanisms of biofilm resistance to antimicrobial agents. *Trends Microbiol*, 9(1): 34-39.

Melo, L.F., 2005. Biofilm physical structure, internal diffusivity and tortuosity. *Water Sci Technol*, 52(7): 77-84.

Middleman, S. (1998) An Introduction to Fluid Dynamics: Principles of Analysis and Design, Academic Press, New York, USA.

Mitchell, A.C., Dideriksen, K., Spangler, L.H., Cunningham, A.B. and Gerlach, R., 2010. Microbially Enhanced Carbon Capture and Storage by Mineral-Trapping and Solubility-Trapping. *Environ Sci Technol*, 44(13): 5270-5276.

Peck, O.P.W., John Chew, Y.M., Bird, M.R. and Bolhuis, A., 2015. Application of Fluid Dynamic Gauging in the Characterization and Removal of Biofouling Deposits. *Heat Transfer Engineering*, 36(7-8): 685-694.

Pelleïeux, S., Bertrand, I., Skali-Lami, S., Mathieu, L., Francius, G. and Gantzer, C., 2012. Accumulation of MS2, GA, and Qβ phages on high density polyethylene (HDPE) and drinking water biofilms under flow/non-flow conditions. *Water Res*, 46(19): 6574-6584.

Rochex, A., Godon, J.-J., Bernet, N. and Escudié, R., 2008. Role of shear stress on composition, diversity and dynamics of biofilm bacterial communities. *Water Res*, 42(20): 4915-4922.

Salley, B., Gordon, P.W., McCormick, A.J., Fisher, A.C. and Wilson, D.I., 2012. Characterising the structure of photosynthetic biofilms using fluid dynamic gauging. *Biofouling*, 28(2): 159-173.

Simões, L.C., Lemos, M., Pereira, A.M., Abreu, A.C., Saavedra, M.J. and Simões, M., 2011. Persister cells in a biofilm treated with a biocide. *Biofouling*, 27(4): 403 — 411.

Simões, L.C. and Simões, M., 2013. Biofilms in drinking water: problems and solutions. *RSC Adv*, 3(8): 2520-2533.

Simões, M., Pereira, M.O. and Vieira, M.J., 2005. Effect of mechanical stress on biofilms challenged by different chemicals. *Water Res*, 39(20): 5142-5152.

Simões, M., Simões, L.C. and Vieira, M.J., 2009. Species association increases biofilm resistance to chemical and mechanical treatments. *Water Res*, 43(1): 229-237.

Stewart, P.S., 2003. Diffusion in biofilms. *J Bacteriol*, 185(5): 1485-1491.

Stewart, P.S. and Franklin, M.J., 2008. Physiological heterogeneity in biofilms. *Nat Rev Microbiol*, 6(3): 199-210.

Tuladhar, T.R., Paterson, W.R., Macleod, N. and Wilson, D.I., 2000. Development of a novel non-contact proximity gauge for thickness measurement of soft deposits and its application in fouling studies. *The Canadian Journal of Chemical Engineering*, 78(5): 935-947.

Whitehead, K.A. and Verran, J., 2006. The Effect of Surface Topography on the Retention of Microorganisms. *Food Bioprod Process*, 84(4): 253-259.

Xu, K.D., McFeters, G.A. and Stewart, P.S., 2000. Biofilm resistance to antimicrobial agents. *Microbiology*, 146(3): 547-549.

Yang, Q., Ali, A., Shi, L. and Wilson, D.I., 2014. Zero discharge fluid dynamic gauging for studying the thickness of soft solid layers. *J Food Eng*, 127(0): 24-33.

Zacheus, O.M., Iivanainen, E.K., Nissinen, T.K., Lehtola, M.J. and Martikainen, P.J., 2000. Bacterial biofilm formation on polyvinyl chloride, polyethylene and stainless steel exposed to ozonated water. *Water Res*, 34(1): 63-70.